Environmental Science & Technology

Article

pubs.acs.org/est

Green Rust Formation during Fe(II) Oxidation by the Nitrate-Reducing *Acidovorax* sp. Strain BoFeN1

Claudia Pantke,[†] Martin Obst,[†] Karim Benzerara,[‡] Guillaume Morin,[‡] Georges Ona-Nguema,[‡] Urs Dippon,[†] and Andreas Kappler*[,†]

[†]Geomicrobiology, Center for Applied Geosciences, University of Tübingen, Hölderlinstr. 12, 72074 Tübingen, Germany

[‡]Institut de Minéralogie et de Physique des Milieux Condensés, UMR 7590, CNRS, UPMC et IPGP, 4 Place Jussieu, 75005 Paris, France

Supporting Information

ABSTRACT: Green rust (GR) as highly reactive iron mineral potentially plays a key role for the fate of (in)organic contaminants, such as chromium or arsenic, and nitroaromatic compounds functioning both as sorbent and reductant. GR forms as corrosion product of steel but is also naturally present in hydromorphic soils and sediments forming as metastable intermediate during microbial Fe(III) reduction. Although already suggested to form during microbial Fe(II) oxidation, clear evidence for GR formation during microbial Fe(II) oxidation was lacking. In the present study, powder XRD, synchrotron-based XAS, Mössbauer spectroscopy, and TEM demonstrated unambiguously the formation of GR as an intermediate product during Fe(II) oxidation by the nitrate-reducing Fe(II)-oxidizer *Acidovorax* sp. strain BoFeN1. The spatial distribution and Fe redox-state of the precipitates associated with the cells were visualized by STXM. It showed the presence of extracellular Fe(III), which can be explained by Fe(III) export from the cells or extracellular Fe(II) oxidation by an oxidant diffusing from the cells. Moreover, GR can be oxidized by nitrate/nitrite and is known as a catalyst for oxidation of dissolved Fe(II) by nitrite/nitrate and may thus contribute to the production of extracellular Fe(III). As a result, strain BoFeN1 may contribute to Fe(II) oxidation and nitrate reduction both by an direct enzymatic pathway and an indirect GR-mediated process.

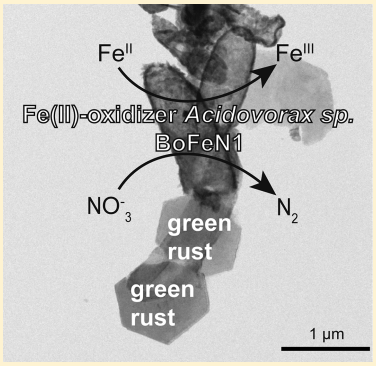

INTRODUCTION

Fe(II)-oxidizing bacteria play an essential role in the redox cycling of iron in both oxic and anoxic environments.[1,2] However, the mechanisms and intermediate Fe minerals formed during microbial Fe(II) oxidation and Fe(III) mineral precipitation, as well as the environmental consequences for the sequestration and transformation of contaminants and nutrients, are barely understood (e.g., refs 3,4). Under oxic conditions microbial Fe(II) oxidation competes with abiotic Fe(II) oxidation.[5] Under anoxic conditions and at neutral pH, dissolved Fe(II) can be oxidized abiotically by manganese oxides and nitrite,[6,7] while Fe(II) in green-rust (GR) is known to be oxidized by both nitrate[8] and nitrite.[9] However, microbial oxidation of dissolved Fe(II) either coupled to the reduction of nitrate or using light energy is the main process for the formation of Fe(III) precipitates under anoxic conditions.[1,10,11] Straub et al.[12] and Hafenbradl et al.[13] identified microorganisms that are able to directly couple Fe(II) oxidation to nitrate reduction. About a decade later, the nitrate-reducing Fe(II)-oxidizing *Acidovorax* strain BoFeN1 was isolated from Lake Constance sediments[14] and a closely related strain was isolated from arsenic-contaminated aquifers in Bangladesh.[15] For *Acidovorax* sp. strain BoFeN1 the spatial association of the cells with the Fe(III) minerals that are precipitated during Fe(II) oxidation, the temporal development of mineral formation, coprecipitation of toxic metal and metalloid ions (arsenic), and the growth benefits of Fe(II) oxidation for the cells have been described.[16−19] It was shown that biomineralization starts within the periplasm of BoFeN1 and that some extracellular Fe-phosphate precipitation occurs in P-rich culture growth medium[20] while in P-poor medium goethite was formed.[17,18]

Generally, geochemical conditions, e.g., pH, the presence of carbonate, phosphate, mineralogical nucleation sites, and other metal ions strongly influence the mineralogy of the precipitates formed during microbial Fe(II) oxidation.[17,21,22] Depending on these conditions, the microbial formation of poorly crystalline ferrihydrite-type minerals, Fe(III) phosphates as well as crystalline minerals such as goethite, lepidocrocite, and magnetite, has been described.[1,14,20,23−25]

In one study GR has been suggested to form during microbial Fe(II) oxidation (by *Dechlorosoma suillum*). However, it was only tentatively identified based on the presence of a few weak X-ray diffraction peaks at high 2θ values and none of the main peaks of GR at 100%, 80%, and 60% intensity.[23] In contrast, microbial GR formation has been described for several Fe(III)-reducing strains.[26−28] GR are mixed Fe(II)−Fe(III)

Received: May 14, 2011
Revised: December 9, 2011
Accepted: December 22, 2011
Published: December 22, 2011

hydroxides with a general formula of $[Fe^{II}_{1-x}Fe^{III}_{x}(OH)_2]^{x+}*[(x/n)A^{n-}*(m/n)H_2O]^{x-}$ (e.g., ref 31). The crystal structure of GR can be described as consisting of brucite-like layers, i.e., hydroxide layers alternating with anion and water molecules as interlayers.[29,30] Bernal et al.[29] first classified GRs in two types: GR one (GR1) incorporating planar or spherical anions such as carbonate or chloride[30] and GR two (GR2) incorporating anions with a more three-dimensional structure such as sulfate. GRs show different Fe(II)/Fe(III) ratios depending on the mechanism of synthesis.[31,32] GRs are naturally found in hydromorphic soils, e.g., fougerite,[33−35] and potentially act as sorbents and reductants for contaminants such as nitrate, selenium, chromium, and etc.[9,36−39]

Several mechanisms for synthetic GR formation have been proposed so far, including solid-state transformation of ferrihydrite by Fe^{2+} [8,40] and controlled oxidation of ferrous hydroxide in the presence of intercalating anions.[36] GR formation by Fe(II)-oxidizing bacteria should thus be possible. Based on these knowledge gaps described above, the objectives of this study were (i) to determine the identity and stability of transient and final Fe mineral phases (with a focus on green rust) formed by *Acidovorax* sp. strain BoFeN1 during oxidation of dissolved Fe(II) at low phosphate concentrations and (ii) to map the spatial distribution of Fe-minerals and their corresponding redox-states around BoFeN1 cells.

MATERIALS AND METHODS

Bacterial Strain and Cultivation Conditions. Experiments were performed with the anaerobic chemoorganotrophic, nitrate-reducing ß-Proteobacterium strain BoFeN1, closely related to *Acidovorax* sp. The bacteria were grown mixotrophically, oxidizing ferrous iron and using acetate as organic cosubstrate for assimilation and energy generation by oxidizing it to CO_2.[14,19] During mixotrophic growth with Fe(II)/acetate and nitrate as electron acceptor, low concentrations of nitrite appeared in the growth medium.[14,19] For cultivation of strain BoFeN1, 10 mM $FeCl_2$, 10 mM Na-nitrate, and 5 mM Na-acetate were added to freshwater mineral medium[18,41] with a reduced phosphate concentration of 1 mM. The composition of the mineral medium was as follows: 0.14 g L^{-1} KH_2PO_4, 0.2 g L^{-1} NaCl, 0.3 g L^{-1} NH_4Cl, 0.5 g L^{-1} $MgSO_4{\cdot}7\ H_2O$, 0.1 g L^{-1} $CaCl_2{\cdot}2\ H_2O$, 1 mL L^{-1} vitamin solution, 1 mL L^{-1} trace element solution, 1 mL L^{-1} selenate−tungstate solution, and 22 mM bicarbonate buffer, pH 6.8−7.2, and the headspace was flushed with N_2/CO_2 (80/20). The addition of the $FeCl_2$ led to precipitation of a white−gray precipitate consisting of Fe(II) phosphate and Fe(II) carbonate.[24] To exclude the presence of background Fe(II) minerals before Fe(II) oxidation and Fe mineral precipitation started, the medium was filtered before inoculation following the protocols of Hohmann et al.[17] and of Kappler and Newman[24] resulting in approximately 6 mM dissolved Fe(II) and approximately 10−20 μM phosphate remaining in the medium. This medium stayed free of Fe(II) precipitates for several weeks in the absence of Fe(II)-oxidizing bacteria which allowed identification of the biotically precipitated Fe(III)-bearing minerals. Five percent of a freshly grown (~3−5 days old) acetate/nitrate (without Fe(II)) grown culture of strain BoFeN1 was added as inoculum. The cultures were incubated at 28 °C in the dark.

Mineralogical and Spectroscopic Analyses. The mineral species formed at the early stage of Fe(II) oxidation were identified by combining transmission electron microscopy (TEM), powder X-ray diffraction (XRD), extended X-ray absorption fine structure (EXAFS) spectroscopy, and Mössbauer spectroscopy. For TEM, 1 mL of culture suspension was taken in the anoxic glovebox (100% N_2), centrifuged and rinsed with deionized water, the supernatant was discarded, and about 1 μL of suspension was deposited onto a Formvar-coated TEM grid. The grids were dried within the glovebox. Dry grids were then transferred to the microscope vacuum chamber. TEM analyses were performed using a JEOL 2100F TEM.

For XRD and EXAFS analysis at the Fe K-edge, samples were collected after 2 days of incubation by filtration (Steritop-GP 0.22 μm, PES, Millipore) and vacuum-dried at room temperature. For XRD, dry powder samples were filled in 0.5-mm diameter glass capillary tubes sealed within a glovebox under anoxic conditions. XRD data were collected using an X'Pert Pro MPD Panalytical diffractometer in Debye−Scherrer transmission geometry. For EXAFS dry powders were pressed to a powder tablet under anoxic conditions within an anoxic glovebox. Special care was taken to maintain anoxic conditions during sample transfer to the beamline and analysis, according to procedures reported in refs 16,17,42, and 43. EXAFS data at the Fe K-edge were collected at 10 K under He atmosphere at bending-magnet beamline BM29 at the ESRF in transmission detection mode using Si(111) double crystal monochromator. EXAFS data were extracted following classical procedures[42,43] and analyzed by linear combination least-squares fitting (LCF) as described in 17. For this fitting procedure our set of iron model compounds included especially goethite, akaganeite, maghemite, ferrihydrite,[44] lepidocrocite, biogenic hydroxycarbonate GR, magnetite,[42] $Fe(OH)_2$,[43] vivianite, and amorphous ferric iron phosphate.[16]

For Mössbauer spectroscopy analysis, the medium was spiked with ^{57}Fe (25 μL of a 1 mM ^{57}Fe(II) stock solution[45]) to improve the quality of the data. To minimize mineral aging, the samples were analyzed directly after sampling. For the analysis, 15 mL of a 2-day-old culture suspension was filtered (0.45 μm, cellulose acetate, Millipore). The wet filters were sealed between two layers of Kapton tape under anoxic conditions. These samples were then mounted on a closed-cycle exchange-gas cryostat (Janis, USA) that allowed cooling of the sample to a set temperature (±0.5 K). Mössbauer spectra were collected with a constant acceleration drive system in transmission mode and with a ^{57}Co source. Spectra were calibrated against a spectrum of alpha-Fe metal foil collected at room temperature. Spectral calibration and fitting was performed with Recoil software (University of Ottawa, Canada) using Voigt-based spectral line shapes. The half width half-maximum value (HWHM) was fixed at 0.097 mm/s for modeling.

For XANES at the Fe $L_{2,3}$-edges and scanning transmission X-ray microscopy (STXM) analyses, samples were collected at two different time points (6 h after incubation and after 1 week). Small aliquots were sampled, centrifuged, and rinsed with deionized water, sandwiched between two Si_3N_4 windows and sealed with epoxy under anoxic conditions in the glovebox. The samples were analyzed with STXM on beamline 10-ID-1 at the Canadian Light Source. Image stacks were acquired across the C-1s and the Fe-2p edges with a spectral resolution of 0.1 eV in the energy regions of interest.[20] The program aXis2000[46] was used for fitting the stacks using a singular value decomposition algorithm for linear decomposition of XANES spectra at the $L_{2,3}$-edges. Calculations for the quantitative species maps were done according to 47. In brief, the image

sequences across the Fe $L_{2,3}$ edges were converted from transmission to linear absorbance (optical density, OD) scale. The resulting spectra at each pixel are then fitted by a linear combination of reference compounds (GR, goethite, and a modeled, nonspecific background, fitted as CH_2O based on the atomic scattering factors[48]). The Fe-reference compounds were selected based on the results of the bulk measurements by EXAFS and Mössbauer spectroscopy since the slight differences of the XAS spectra of the STXM measurements at the Fe $L_{2,3}$ edge would not allow for an unambiguous identification of the Fe-mineral phase. The goethite sample used as reference for this analysis was synthesized according to the procedure reported by Juillot et al.[49] The sample of hydroxycarbonate green-rust, GR(CO_3), used in the present study as reference for XANES analysis at the $L_{2,3}$-edges as well as for EXAFS analysis at the Fe K-edge was synthesized from the reduction of lepidocrocite by *Shewanella putrefaciens* strain ATCC 12099 and characterized as described in the paper by Ona-Nguema et al.[28]

RESULTS

Morphology and Identity of Fe Minerals Formed by BoFeN1. XRD analysis (Figure 1), EXAFS analysis (Figure 2), and TEM observations (Figure 3), as well as Mössbauer spectroscopy analysis (Figure 4), of precipitates formed by the nitrate-reducing Fe(II)-oxidizer BoFeN1 within 2 days of incubation (after oxidation of ~2 mM of the initial ~6 mM Fe(II)) demonstrate that they consist of a mixture of the major compounds goethite and GR(CO_3). In particular XRD analysis of the 2-d BoFeN1 sample under anoxic condition revealed that the *d*-spacings at d_{003} = 0.753 nm, d_{006} = 0.376 nm, d_{012} = 0.267 nm, d_{015} = 0.235 nm, and d_{018} = 0.197 nm correspond to those of GR(CO_3), as previously shown by Ona-Nguema et al.[28,50] for biogenic GR(CO_3) formed during bioreduction of lepidocrocite. Accordingly, LCF of EXAFS data reveals that GR(CO_3) accounts for 25 ± 10% of the total iron after 2 days (Figure 2). Indeed, the best fit was obtained when including the spectra of small particle goethite[44] and biogenic GR(CO_3) as fitting components. This is especially obvious at the strong shoulders exhibited at 8.5 and 9 K of the experimental data of the LCF analysis (Figure 2A). Comparison of the fitting results obtained using GR(CO_3) and GR(Cl) is reported in Figure S1, showing that the best fit is obtained with GR(CO_3). The sum of the components was 88% for this best fit, which is below 100%. However, as illustrated in Figure S1, addition of any other component including GR(Cl), magnetite Fe_3O_4, vivianite [$Fe_3(PO_4)_2{\cdot}8H_2O$], amorphous ferric phosphate,[20] ferrihydrite, or other Fe(III) (oxyhydr)oxides than goethite[44] did neither improve the fit nor the sum of the fitting components. XRD analysis indicated the absence of siderite, Fe(CO_3), but revealed the presence of minor amount of bobierrite, $Mg_3(PO_4)_2{\cdot}8H_2O$, that could have formed from precipitation of Mg^{2+} and phosphate ions present in the culture medium. Consequently, although the absence of vivianite is confirmed by EXAFS analysis, the presence of Fe(II) substituted for Mg(II) in the bobierrite structure could account for the discrepancy observed on the sum of our EXAFS components. Further synthesis of such model compounds would be required to check this hypothesis. Alternatively, this discrepancy on the sum of the LCF components could rely on the difficulty to reproduce the low amplitude spectrum of the biogenic goethite component compared to that of bulk goethite, even using our small particle goethite model compound. It could also be due to possible differences in the Fe(II)/Fe(III) ratio in our GR(CO_3) model compound compared to the biogenic one produced by BoFeN1. When normalized to a sum of 100%, the GR(CO_3) and goethite components can be estimated as 25 ± 10% and 75 ± 10%, respectively.

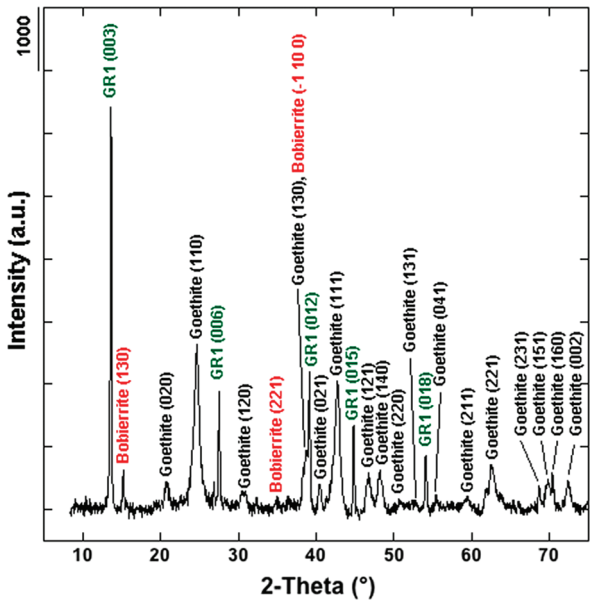

Figure 1. X-ray powder diffraction pattern of biogenic Fe-bearing minerals produced upon Fe(II) oxidation by the nitrate-reducing *Acidovorax* sp. strain BoFeN1 after 2 days of incubation. The diffractogram clearly indicates the presence of hydroxycarbonate green-rust (GR) mixed with goethite and bobierrite [$Mg_3(PO_4)_2{\cdot}8H_2O$]. CoKα radiation (λ = 0.179 nm).

TEM images of BoFeN1 cells and precipitates in samples collected after 2 days of incubation displayed nm-sized globular mineral structures at the cell surface, as already described previously for BoFeN1 cells,[16] plus hexagonal crystals with a diameter of ~1 μm (Figure 3). After 6 h of incubation hexagonal crystals were not well developed compared to the samples collected after 2 days of incubation (Supporting Information Figure S5). Similar hexagonal structures with a diameter of ~2 μm were described and identified as GR by McGill.[51] The diameter of the particles was shown to be influenced by the synthesis method, the age of the crystal particle, and the Fe(III)-reducing bacterial strain involved in GR formation.[52−54] Continuous growth and aging during precipitation of GR either by chemical synthesis or formation by Fe(III)-reducing bacteria forms larger crystals (particle size of a few μm)[28,52,53] compared to synthesis by rapid Fe(II) oxidation, e.g., by H_2O_2, or by coprecipitation of Fe^{2+} and Fe^{3+} ions, that lead to small particle size of several hundred nm.[55,56] The hexagonal plates produced by the nitrate-reducing Fe(II)-oxidizing strain BoFeN1 have a diameter of ~1 μm (Figure 3) which correlates well with the size of GR crystals measured in other studies where precipitation during bacterial Fe(III) reduction by *Shewanella* sp. was used as synthesis mechanism.[28,52,54]

Finally, Mössbauer spectroscopy analysis of BoFeN1 precipitates collected after 2 days of incubation from cultures that were spiked with ^{57}Fe(II) (Figure 4) confirmed TEM and EXAFS analyses at the Fe K-edge. The dominant component of the Mössbauer spectrum measured at 77 K (Table S1) was

dx.doi.org/10.1021/es2016457 | *Environ. Sci. Technol.* 2012, 46, 1439−1446

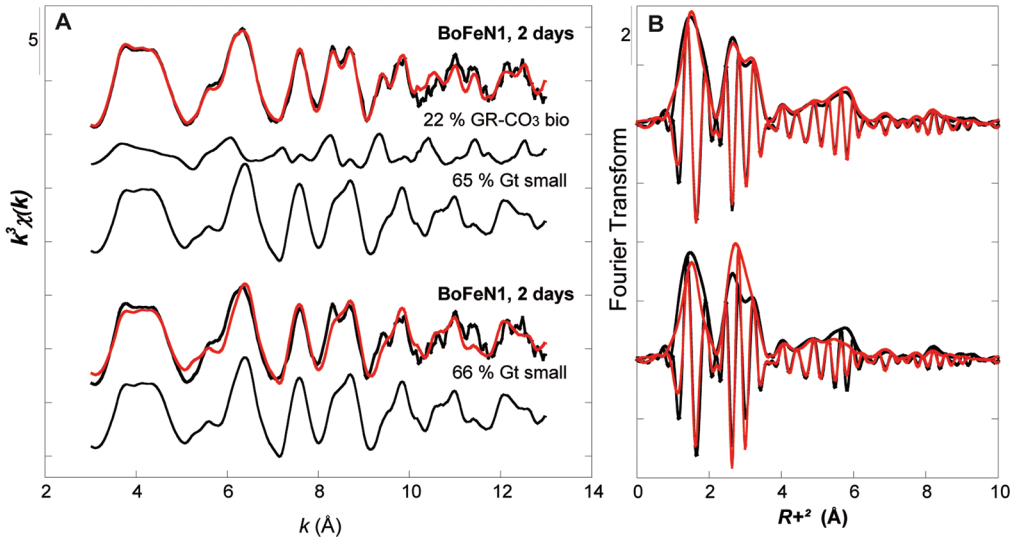

Figure 2. (A) Linear combination fit (LCF) of k^3-weighted EXAFS data obtained at the Fe K-edge for the BoFeN1 sample incubated for two days (BoFeN1, 2 days). Experimental data and fit curves are displayed in black and red, respectively, and fit components are given below the data and fit curves. Data obtained for BoFeN1 precipitated collected after 2 days were modeled either by a combination of small particle goethite and biogenic GR (top) or by goethite alone (bottom). Note the strong shoulders at 8.5 and 9 K. (B) Comparison of fits of Fourier-transformed data either including (top) or not including (bottom) GR indicates that GR is a significant component of the biogenic "BoFeN1, 2 days" sample. The first and second peaks of the FT transform magnitude correspond to the contributions from Fe−O and Fe−Fe backscattering paths, respectively.

goethite, with the goethite sextet covering 70% (% of atomic ^{57}Fe) of the total spectral area. Three doublets with a total area of 24% are assigned to hydroxycarbonate GR according to parameter values reported in 57 and 58 at 77 K (Table S1) for the two crystallographic Fe(II) sites and the Fe(III) site in GR(CO_3). This biogenic green-rust has an Fe(II)/Fe(III) ratio of 2.5 (Table S1) in agreement with the ratio reported by Murad and Taylor[59] for GR(CO_3), i.e., between 2 and 3. The fit is further improved by including an additional Fe(III) doublet with an area of 6%, which may correspond to a poorly crystalline superparamagnetic Fe(III) oxyhydroxide phase such as, e.g., ferrihydrite or nanogoethite.

Spatial Distribution of Fe Precipitates and BoFeN1 Cells. STXM which combines XANES with high spatial resolution microscopy (in this study approximately 50 nm) allows an elemental-edge based discrimination between elements, their redox states, and even different chemical compounds based on their bonding environments. STXM at the Fe $L_{2,3}$-edges was used for analyzing the spatial distribution of Fe mineral precipitates formed by strain BoFeN1 6 h (Figure 5) and 1 week after inoculation (Supporting Information S3). Interestingly, we frequently identified very fine pre-edge structures on the L_3 edges at around 705.6, 706.0, and 706.3 eV and on the L_2 edge at around 718.6 eV on spectra measured on 6 h samples (Figure 5F). These features are visible only in the spectrum of reference GR whereas they are absent from all the spectra of reference Fe(III) (oxy)hydroxides and Fe(II) carbonate (data not shown). Figure 5F shows an average spectrum typical of what is measured on 6 h samples and the corresponding fit using a linear combination of GR and goethite reference spectra selected according to EXAFS, TEM, and Mössbauer data. The relative energy position of the peaks which is a major parameter in XANES spectra at the $L_{2,3}$ edges (e.g., explained for the Fe-$L_{2,3}$-edge in ref 60) is well explained by the spectra of the reference compounds at both the L_2 and L_3 edges. The absolute energy position at the Fe $L_{2,3}$ edges cannot be determined precisely since in this energy region no gas spectra are available for energy calibration. However, this is not a problem for data analysis as all data are treated equally. In contrast to the energy position, the relative intensity of the different peaks is slightly different. One reason might be that the Fe(II)/Fe(III) ratio is not the same in the reference GR(CO_3) we used and in the GR(CO_3) formed by strain BoFeN1 within 6 h after inoculation. Average C-1s spectra of GR-rich regions in the 6 h sample clearly show a pronounced absorption peak at 290.3 eV (Supporting Information Figure S2) characteristic of carbonate groups, thus giving evidence for the presence of GR(CO_3) in this 6 h sample. GR and goethite STXM maps were fitted using spectra of reference compounds. Maps showed that GR(CO_3) was present in the vicinity of cells (between cells) as well as in association with the cells (Figure 5A and C). In the 6 h sample, goethite was identified in the vicinity of the cells but also to a large extent associated with the cell surfaces (Figure 5B and C). One week old samples showed an advanced oxidation state of the iron precipitates with almost exclusively goethite precipitates associated with the cells (Supporting Information Figure S3).

DISCUSSION

Mechanism of Green Rust Formation by BoFeN1. The finding of Fe(III) associated with GR in the extracellular environment of neutrophilic Fe(II)-oxidizing cells rises the question regarding the Fe(II) oxidation process or processes in this system. In cultures of Fe(III)-reducing bacteria, dissolved Fe(II) produced by cells reacts with remaining nondissolved Fe(III) that is initially present in the extracellular medium to form GR.[28,54,61] *Acidovorax* sp. BoFeN1 was shown to enzymatically oxidize Fe(II).[19] The presence of Fe(III) away from Fe(II)-oxidizing bacteria is somewhat surprising given the low solubility of Fe(III) at neutral pH.[62] Several nonexclusive hypotheses can be proposed: (1) Fe(II) is oxidized in the periplasm of BoFeN1 then exported extracellularly. This would be favored by a local pH drop (as suggested, e.g., in ref 24), cell lysis, or the formation of an inorganic aqueous complex and/or

dx.doi.org/10.1021/es2016457 | Environ. Sci. Technol. 2012, 46, 1439−1446

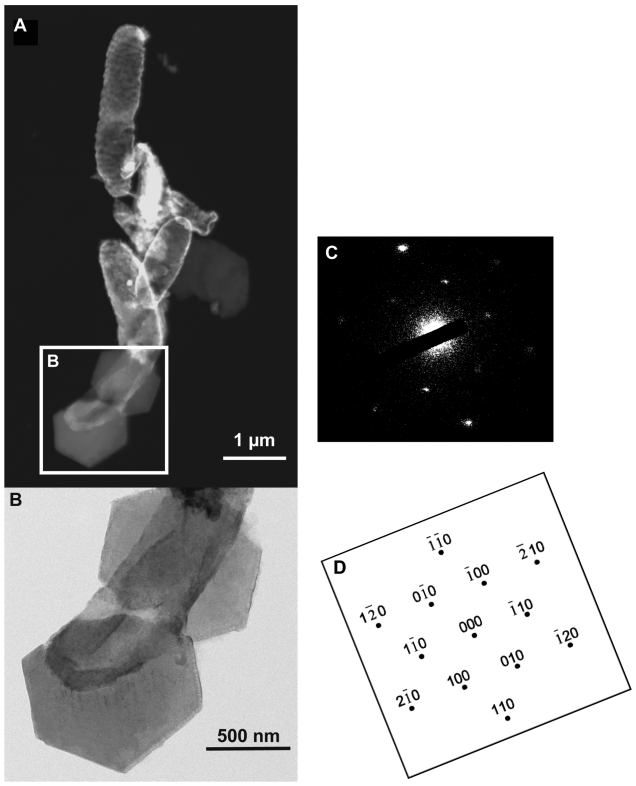

Figure 3. Scanning transmission electron microscopy (STEM) image of BoFeN1 culture suspension after 2 days measured in the high angular annular dark field mode (HAADF) (A). Magnified transmission electron microscopy image of BoFeN1 cell with hexagonal carbonate GR flakes measured in brightfield mode (B). Selected area electron diffraction (SAED) pattern on a single GR particle oriented along the [001] zone axis (C). The electron diffraction pattern is composed of spots distributed on a hexagonal lattice. The cell parameters deduced from the diffraction patterns are $a = b = 3.12$ Å in agreement with the GR structure.[77] A calculated diffraction pattern is provided (D).

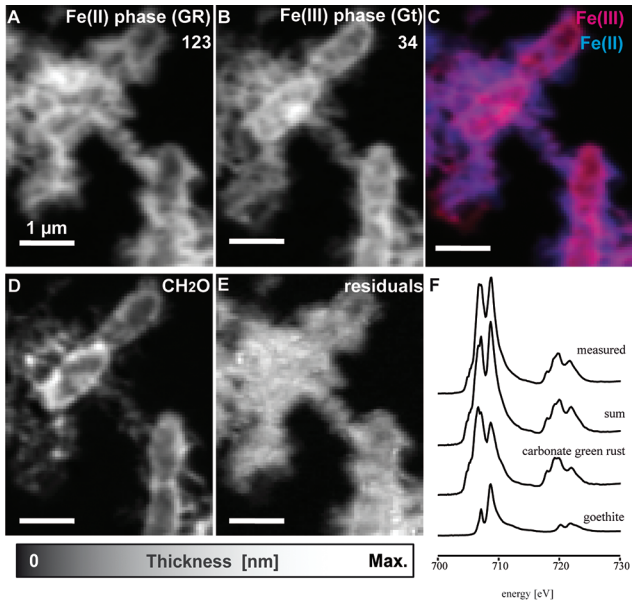

Figure 5. STXM data for a BoFeN1 culture suspension collected after 6 h of incubation. Quantitative species maps of the Fe(II)- and Fe(III)-containing compounds of the cell−mineral aggregates, calculated from spectromicroscopic STXM measurements (A, B). The values, e.g., 123 nm, noted beneath the labeling Fe(II) or Fe(III) give the maximum cumulative thickness (white) of the respective compounds. The spatial arrangement of the individual compounds is shown in a color overlay (C). Fe(II) and Fe(III) maps have been modeled using carbonate GR and goethite as reference, respectively (A, B, C). The non-Fe-background was fitted as CH_2O (D). The residuals are displayed (E). Linear combination fit of an average spectrum (measured) of extracellular precipitate (6 h sample), including carbonate green rust and goethite as fitting components, as well as the summarized fit (sum), all on linear absorbance scale (F).

as a colloidal aggregate as suggested by Miot et al.[16] (2) Some Fe(II) is oxidized extracellularly (in addition to Fe(II) oxidation in the cells) by nitrite/nitrate (probably also catalyzed by green rust), see Discussion below. The nitrite concentration usually observed in cultures of the nitrate-reducing Fe(II)-oxidizer strain BoFeN1 is 1.0−1.5 mM after the beginning of Fe(II) and acetate consumption.[14] This latter hypothesis has been proposed by Miot et al.[16] Indeed, these authors followed the spatial and temporal evolution of the Fe redox state of the nitrate-reducing Fe(II)-oxidizer BoFeN1 in growth medium that contained a higher phosphate concentration compared to

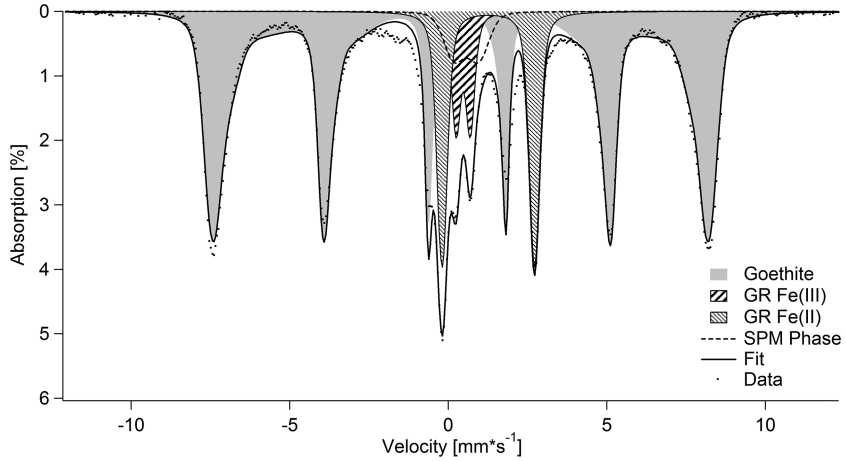

Figure 4. Mössbauer spectrum (measured at 77 K) of BoFeN1 precipitates formed in growth medium that was spiked with ^{57}Fe(II) (Mössbauer spectroscopy parameters are provided in Table S1). Precipitates were sampled after 2 days of incubation. Goethite (GT) − gray sextet, green rust (GR) with GR Fe(III) and GR Fe(II) doublets, superparamagnetic phase (SPM) − dashed line.

dx.doi.org/10.1021/es2016457 | Environ. Sci. Technol. 2012, 46, 1439−1446

the present study (4.4 mM compared to 1 mM phosphate; values before filtration of growth medium) and described a gradual oxidation of Fe(II) leading to the formation of an amorphous Fe(III)−phosphate mineral phase. However, they did not detect GR although they could observe a greenish intermediary precipitate after 4 days. This greenish precipitate was interpreted in their study as a mixed valence Fe(II)−Fe(III) phosphate. The difference from their study to what we observed here is most likely due to the phosphate concentration that is significantly lower in our experiments and thus prevented the formation of Fe(II)−Fe(III) phosphate minerals.

Implications of GR Formation by Fe(II)-Oxidizing Bacteria. GR might serve as an intermediate compound[28,63,64] that is then transformed to goethite through further Fe(II) oxidation (Supporting Information S4). Although discrimination between a solid-state transformation of GR or transformation in the presence of a fluid phase by interface-coupled dissolution-reprecipitation[65] is beyond the scope of this paper, we have evidence that templating effects sometimes occur preserving the morphology of hexagonal GR platelets, e.g., goethite needle growth on the edge of hexagonal GR platelets (Supporting Information Figure S4). Various minerals, e.g., ferrihydrite, goethite, akaganeite, lepidocrocite, hematite, and maghemite as well as magnetite, have been described to form during abiotic as well as biotic oxidation of GR.[23,39,62,66] Oxidation of Fe(II) in GR might be due to reaction with nitrate present in the growth medium and/or nitrite that can be produced by BoFeN1 cells (e.g., 14 and 16).

Interestingly, it has been shown previously[8,9] that GR can catalyze oxidation of dissolved Fe(II) by reduction of nitrate and/or nitrite. This process might explain part of the Fe(II) oxidation occurring in the extracellular growth medium of BoFeN1. All these results can be reconciled in the following scenario: BoFeN1 cells oxidize Fe(II) into Fe(III) in their cell wall and produce some nitrite. Some Fe(III) might form extracellularly at a slow rate by nitrite-coupled Fe(II) oxidation. The formation of GR then occurs extracellularly as shown in this study. GR then catalyzes further Fe(II) oxidation extracellularly by reducing nitrate and nitrite leading to the formation of goethite. GR thus could play a crucial role as catalyst for extracellular Fe(II) oxidation by nitrite/nitrate. Overall, this suggests that there may be a direct cell-membrane-associated role of BoFeN1 cells in the oxidation of Fe(II) in parallel with an indirect extracellular and GR-catalyzed role. The relative proportion of each process in the oxidation of Fe(II) has yet to be quantified precisely. Furthermore, this study sets a stage for future experiments with anaerobic and aerobic Fe(II)-oxidizing bacteria where progressive Fe(II) oxidation and secondary mineral formation can be explored, including a thorough understanding of why goethite is the stable end product, e.g., as described by Drissi et al.,[58] under these geochemical conditions.

More generally, GRs are highly reactive Fe mineral phases in many environments including soils, sediments, and permeable reactive barrier systems.[33,35,67,68] They were often described as reductants for several contaminants, e.g., carbon tetrachloride,[69] nitrate and nitrites,[8,9] selenium,[70,71] chromium,[37−39] and uranium[72], but also gold, silver, copper, and mercury.[73] Additionally, isomorphic substation of Fe^{2+} by incorporating divalent cations has been described so far for nickel as well as for zinc, cadmium, cobalt, and magnesium.[27,74,75] All these mechanism may influence the (im)mobilization of contaminants, e.g., removal of nitrate from water or agricultural soil through GR enhanced reduction to ammonium.[8,9,55] For arsenic, the formation of arsenate- as well as arsenite-inner-sphere complexes with GR rather than arsenate reduction to arsenite and thus a potential mobilization and increase in As toxicity have been described.[64,76] This is of special interest as the nitrate-dependent Fe(II)-oxidizer BoFeN1 used in this study is closely related to an *Acidovorax* strain recently identified in an As-contaminated aquifer.[15] Strain BoFeN1 was also shown to effectively immobilize arsenic from solution by adsorption and coprecipitation.[17,18]

Overall the present study extends the range of possible processes forming reactive GRs further enhancing the potential importance of GRs as reactive species for contaminant transformation. Additionally, the present study illustrates the importance of analysis of minerals formed during the course of microbial (or chemical) Fe(II) oxidation and shows that it is not sufficient to identify and characterize the end products of this oxidation process since many highly reactive minerals will be overlooked, although they might readily influence the fate of contaminants.

■ ASSOCIATED CONTENT

Supporting Information

Table S1 and Figures S1−S5. This material is available free of charge via the Internet at http://pubs.acs.org.

■ AUTHOR INFORMATION

Corresponding Author

*Phone: +49-7071-2974992; fax: +49-7071-295059; e-mail: andreas.kappler@uni-tuebingen.de.

■ ACKNOWLEDGMENTS

This work was supported by a research proposal (KA 1736/14-1) from the German Research Foundation (DFG) and by the project "MicroActiv" of the BMBF/DFG program "Geotechnologien" to AK, and by a BMBF IPSWaT fellowship to C.P. and U.D. The work done by G.M. was funded by EC2CO-CYTRIX CNRS/INSU program, by ACI/FNS grant 3033, and by SESAME IdF grant 1775. The synchrotron-based STXM research was supported by the Emmy-Noether program of the DFG to M.O. (OB 362/1-1) and the Interrvie program of the INSU to K.B. Research described in this paper was performed at the Canadian Light Source, which is supported by the Natural Sciences and Engineering Research Council of Canada, the National Research Council Canada, the Canadian Institutes of Health Research, the Province of Saskatchewan, Western Economic Diversification Canada, and the University of Saskatchewan. The JEOL JEM-2100F at IMPMC was supported by Region Ile-de-France grant SESAME 2000 E 1435, INSU-CNRS, INP-CNRS, and University Pierre et Marie Curie − Paris 6.

■ REFERENCES

(1) Weber, K. A.; Achenbach, L. A.; Coates, J. D. Microorganisms pumping iron: Anaerobic microbial iron oxidation and reduction. *Nat. Rev. Microbiol.* **2006**, *4* (10), 752−764.

(2) Schmidt, C.; Behrens, S.; Kappler, A. Ecosystem functioning from a geomicrobiological perspective − a conceptual framework for biogeochemical iron cycling. *Environ. Chem.* **2010**, *7* (5), 399−405.

(3) Schaedler, S.; Burkhardt, C.; Hegler, F.; Straub, K. L.; Miot, J.; Benzerara, K.; Kappler, A. Formation of cell-iron-mineral aggregates by

phototrophic and nitrate-reducing anaerobic Fe(II)-oxidizing bacteria. *Geomicrobiol. J.* **2009**, *26*, 93−103.
(4) Benzerara, K.; Miot, J.; Morin, G.; Skouri-Panet, F.; Férard, C. Significance, mechanisms and environmental implications of microbial biomineralization. *C. R. Geosci.* **2011**, *343*, 160−167.
(5) Neubauer, S. C.; Emerson, D.; Megonigal, J. P. Life at the energetic edge: Kinetics of circumneutral iron oxidation by lithotrophic iron-oxidizing bacteria isolated from the wetland-plant rhizosphere. *Appl. Environ. Microbiol.* **2002**, *68* (8), 3988−3995.
(6) Myers, C. R.; Nealson, K. H. Microbial reduction of manganese oxides: Interactions with iron and sulfur. *Geochim. Cosmochim. Acta* **1988**, *52* (11), 2727−2732.
(7) Moraghan, J.; Buresh, R. Chemical reduction of nitrite and nitrous oxide by ferrous iron. *Soil. Sci. Soc. Am. J.* **1977**, *41*, 47−50.
(8) Hansen, H. C. B.; Borggaard, O. K.; Sørensen, J. Evaluation of the free energy of formation of Fe(II)-Fe(III) hydroxide-sulphate (green rust) and its reduction of nitrite. *Geochim. Cosmochim. Acta* **1994**, *58* (12), 2599−2608.
(9) Hansen, H. C. B.; Koch, C. B.; Nancke-Krogh, H.; Borggaard, O. K.; Sørensen, J. Abiotic nitrate reduction to ammonium: Key role of green rust. *Environ. Sci. Technol.* **1996**, *30* (6), 2053−2056.
(10) Kappler, A.; Straub, K. L. Geomicrobiological cycling of iron. *Rev. Mineral. Geochem.* **2005**, *59* (1), 85−108.
(11) Konhauser, K. O.; Kappler, A.; Roden, E. E. Iron in microbial metabolism. *Elements* **2011**, *7* (2), 89−93.
(12) Straub, K. L.; Benz, M.; Schink, B.; Widdel, F. Anaerobic, nitrate-dependent microbial oxidation of ferrous iron. *Appl. Environ. Microbiol.* **1996**, *62* (4), 1458−1460.
(13) Hafenbradl, D.; Keller, M.; Dirmeier, R.; Rachel, R.; Rossnagel, P.; Burggraf, S.; Huber, H.; Stetter, K. O. *Ferroglobus placidus gen. nov., sp. nov.*, A novel hyperthermophilic archaeum that oxidizes Fe^{2+} at neutral pH under anoxic conditions. *Arch. Microbiol.* **1996**, *166* (5), 308−14.
(14) Kappler, A.; Schink, B.; Newman, D. K. Fe(III) mineral formation and cell encrustation by the nitrate-dependent Fe(II)-oxidizer strain BoFeN1. *Geobiology* **2005**, *3* (4), 235−245.
(15) Sutton, N. B.; van der Kraan, G. M.; van Loosdrecht, M. C. M.; Muyzer, G.; Bruining, J.; Schotting, R. J. Characterization of geochemical constituents and bacterial populations associated with As mobilization in deep and shallow tube wells in Bangladesh. *Water Res.* **2009**, *43* (6), 1720−1730.
(16) Miot, J.; Benzerara, K.; Morin, G.; Bernard, S.; Beyssac, O.; Larquet, E.; Kappler, A.; Guyot, F. Transformation of vivianite by anaerobic nitrate-reducing iron-oxidizing bacteria. *Geobiology* **2009**, *7* (3), 373−384.
(17) Hohmann, C.; Morin, G.; Ona-Nguema, G.; Guigner, J.-M.; Brown, G. E. Jr; Kappler, A. Molecular-level modes of As binding to Fe(III) (oxyhydr)oxides precipitated by the anaerobic nitrate-reducing iron(II)-oxidizing *Acidovorax sp.* strain BoFeN1. *Geochim. Cosmochim. Acta* **2011**, *75* (17), 4699−4712.
(18) Hohmann, C.; Winkler, E.; Morin, G.; Kappler, A. Anaerobic Fe(II)-oxidizing bacteria show As resistance and immobilize As during Fe(III) mineral precipitation. *Environ. Sci. Technol.* **2010**, *44* (1), 94−101.
(19) Muehe, E. M.; Gerhardt, S.; Schink, B.; Kappler, A. Ecophysiology and the energetic benefit of mixotrophic Fe(II) oxidation by various strains of nitrate-reducing bacteria. *FEMS Microbiol. Ecol.* **2009**, *70*, 335−343.
(20) Miot, J.; Benzerara, K.; Morin, G.; Kappler, A.; Bernard, S.; Obst, M.; Férard, C.; Skouri-Panet, F.; Guigner, J.-M.; Posth, N.; Galvez, M.; Brown, G. E. Jr; Guyot, F. Iron biomineralization by anaerobic neutrophilic iron-oxidizing bacteria. *Geochim. Cosmochim. Acta* **2009**, *73* (3), 696−711.
(21) Larese-Casanova, P.; Haderlein, S. B.; Kappler, A. Biomineralization of lepidocrocite and goethite by nitrate-reducing Fe(II)-oxidizing bacteria: Effect of pH, bicarbonate, phosphate, and humic acids. *Geochim. Cosmochim. Acta* **2010**, *74* (13), 3721−3734.
(22) Senko, J. M.; Dewers, T. A.; Krumholz, L. R. Effect of oxidation rate and Fe(II) state on microbial nitrate-dependent Fe(III) mineral formation. *Appl. Environ. Microbiol.* **2005**, *71* (11), 7172−7177.
(23) Chaudhuri, S. K.; Lack, J. G.; Coates, J. D. Biogenic magnetite formation through anaerobic biooxidation of Fe(II). *Appl. Environ. Microbiol* **2001**, *67* (6), 2844−2848.
(24) Kappler, A.; Newman, D. K. Formation of Fe(III)-minerals by Fe(II)-oxidizing photoautotrophic bacteria. *Geochim. Cosmochim. Acta* **2004**, *68* (6), 1217−1226.
(25) Weber, K. A.; Pollock, J.; Cole, K. A.; O'Connor, S. M.; Achenbach, L. A.; Coates, J. D. Anaerobic nitrate-dependent iron(II) bio-oxidation by a novel lithoautotrophic betaproteobacterium, strain 2002. *Appl. Environ. Microbiol.* **2006**, *72* (1), 686−694.
(26) Fredrickson, J. K.; Zachara, J. M.; Kennedy, D. W.; Dong, H.; Onstott, T. C.; Hinman, N. W.; Li, S.-m. Biogenic iron mineralization accompanying the dissimilatory reduction of hydrous ferric oxide by a groundwater bacterium. *Geochim. Cosmochim. Acta* **1998**, *62* (19−20), 3239−3257.
(27) Parmar, N.; Gorby, Y. A.; Beveridge, T. J.; Ferris, F. G. Formation of green rust and immobilization of nickel in response to bacterial reduction of hydrous ferric oxide. *Geomicrobiol. J.* **2001**, *18*, 375−385.
(28) Ona-Nguema, G.; Abdelmoula, M.; Jorand, F.; Benali, O.; Block, J.-C.; Génin, J.-M. R. Iron(II,III) hydroxycarbonate green rust formation and stabilization from lepidocrocite bioreduction. *Environ. Sci. Technol.* **2002**, *36* (1), 16−20.
(29) Bernal F.R.S., J. D.; Dasgupta, D. R.; Mackay, A. L. The oxides and hydroxides of iron and their structural inter-relationships. *Clay Miner. Bull.* **1959**, *4* (21), 15−30.
(30) Keller, G. Über Hydroxyde und basische Salze des 2wertigen Eisens und deren dunkelgrünen Oxydationsprodukte. Ph.D. Dissertation, University Bern, Bern, 1948.
(31) Génin, J.-M. R.; Refait, P.; Bourrié, G.; Abdelmoula, M.; Trolard, F. Structure and stability of the Fe(II)-Fe(III) green rust "fougerite" mineral and its potential for reducing pollutants in soil solutions. *Appl. Geochem.* **2001**, *16* (5), 559−570.
(32) Feitknecht, W.; Keller, G. Über die dunkelgrünen Hydroxyverbindungen des Eisens. *Z. Anorg. Chem.* **1950**, *262* (1−5), 61−68.
(33) Abdelmoula, M.; Trolard, F.; Bourrié, G.; Génin, J. M. R. Evidence for the Fe(II)-Fe(III) green rust "fougerite" mineral occurrence in a hydromorphic soil and its transformation with depth. *Hyperfine Interact.* **1998**, *112* (1), 235−238.
(34) Trolard, F.; Bourrie, G.; Abdelmoula, M.; Refait, P.; Feder, F. Fougerite, a new mineral of the pyroaurite-iowaite group: Description and crystal structure. *Clays Clay Miner.* **2007**, *55* (3), 323−334.
(35) Trolard, F.; Génin, J. M. R.; Abdelmoula, M.; Bourrié, G.; Humbert, B.; Herbillon, A. Identification of a green rust mineral in a reductomorphic soil by Mossbauer and Raman spectroscopies. *Geochim. Cosmochim. Acta* **1997**, *61* (5), 1107−1111.
(36) Génin, J.-M. R.; Abdelmoula, M.; Refait, P. H.; Simon, L. Comparison of the green rust two lamellar double hydroxide class with the green rust one pyroaurite class: Fe(II)±Fe(III) sulphate and selenate hydroxides. *Hyperfine Interact.* **1998**, *C* (3), 313−316.
(37) Williams, A. G.; Scherer, M. M. Kinetics of Cr(VI) reduction by carbonate green rust. *Environ. Sci. Technol.* **2001**, *35* (17), 3488−94.
(38) Bond, D. L.; Fendorf, S. Kinetics and structural constraints of chromate reduction by green rusts. *Environ. Sci. Technol.* **2003**, *37* (12), 2750−2757.
(39) Loyaux-Lawniczak, S.; Refait, P.; Ehrhardt, J.-J.; Lecomte, P.; Génin, J.-M. R. Trapping of Cr by formation of ferrihydrite during the reduction of chromate ions by Fe(II)−Fe(III) hydroxysalt green rusts. *Environ. Sci. Technol.* **1999**, *34* (3), 438−443.
(40) Mann, S.; Sparks, N. H. C.; Couling, S. B.; Larcombe, M. C.; Frankel, R. B. Crystallochemical characterization of magnetic spinels prepared from aqueous solution. *J. Chem. Soc. Faraday Trans. 1* **1989**, *85* (9), 3033−3044.
(41) Hegler, F.; Posth, N. R.; Jiang, J.; Kappler, A. Physiology of phototrophic iron(II)-oxidizing bacteria-implications for modern and ancient environments. *FEMS Microbiol. Ecol.* **2008**, *66*, 250−260.

(42) Morin, G.; Wang, Y.; Ona-Nguema, G.; Juillot, F.; Calas, G.; Menguy, M.; Aubry, E.; Bargar, J. R.; Brown, G. E. Jr. EXAFS and HRTEM evidence for As(III)-containing surface precipitates on nanocrystalline magnetite: Implications for As sequestration. *Langmuir* **2009**, *25*, 9119−9128.
(43) Ona-Nguema, G.; Morin, G.; Wang, Y.; Menguy, N.; Juillot, F. M.; Olivi, L.; Aquilanti, G.; Abdelmoula, M.; Ruby, C.; Bargar, J. R.; Guyot, F.; Calas, G.; Brown, G. E. Jr. Arsenite sequestration at the surface of nano-Fe(OH)2, ferrous-carbonate hydroxide, and green-rust after bioreduction of arsenic-sorbed lepidocrocite by *Shewanella putrefaciens*. *Geochim. Cosmochim. Acta* **2009**, *73*, 1359−1365.
(44) Maillot, F.; Morin, G.; Wang, Y.; Bonnin, D.; Ildefonse, P.; Chaneac, C.; Calas, G. New insight into the structure of nanocrystalline ferrihydrite: EXAFS evidence for tetrahedrally coordinated iron(III). *Geochim. Cosmochim. Acta* **2011**, *75*, 2708−2720.
(45) Williams, A. G. B.; Scherer, M. M. Spectroscopic evidence for Fe(II)-Fe(III) electron transfer at the iron oxide-water interface. *Environ. Sci. Technol.* **2004**, *38* (18), 4782−4790.
(46) Hitchcock, A. P. *aXis2000*, aXis2000 is written in Interactive Data Language (IDL) and available for free for non-commercial use. http://unicorn.mcmaster.ca/aXis2000.html 2009.
(47) Dynes, J. J.; Tyliszczak, T.; Araki, T.; Lawrence, J. R.; Swerhone, G. D. W.; Leppard, G. G.; Hitchcock, A. P. Speciation and quantitative mapping of metal species in microbial biofilms using scanning transmission X-ray microscopy. *Environ. Sci. Technol.* **2006**, *40* (5), 1556−1565.
(48) Henke, B. L.; Gullikson, E. M.; Davis, J. C. X-ray interactions: Photoabsorption, scattering, transmission, and reflection at E = 50−30,000 eV, Z = 1−92. *At. Data Nucl. Data Tables* **1993**, *54* (2), 181−342.
(49) Juillot, F.; Maréchal, C.; Ponthieu, M.; Cacaly, S.; Morin, G.; Benedetti, M.; Hazemann, J. L.; Proux, O.; Guyot, F. Zn isotopic fractionation caused by sorption on goethite and 2-lines ferrihydrite. *Geochim. Cosmochim. Acta* **2008**, *72* (19), 4886−4900.
(50) Ona-Nguema, G.; Carteret, C.; Benali, O.; Abdelmoula, M.; Génin, J.-M.; Jorand, F. Competitive formation of hydroxycarbonate green rust 1 versus hydroxysulphate green rust 2 in *Shewanella putrefaciens* cultures. *Geomicrobiol. J.* **2004**, *21*, 79−90.
(51) McGill, I. R.; McEnaney, B.; Smith, D. C. Crystal structure of green rust formed by corrosion of cast iron. *Nature* **1976**, *259* (5540), 200−201.
(52) Legrand, L.; Abdelmoula, M.; Géhin, A.; Chaussé, A.; Génin, J. M. R. Electrochemical formation of a new Fe(II)-Fe(III) hydroxycarbonate green rust: Characterisation and morphology. *Electrochim. Acta* **2001**, *46* (12), 1815−1822.
(53) Géhin, A.; Ruby, C.; Abdelmoula, M.; Benali, O.; Ghanbaja, J.; Refait, P.; Génin, J.-M. R. Synthesis of Fe(II-III) hydroxysulphate green rust by coprecipitation. *Solid State Sci.* **2002**, *4* (1), 61−66.
(54) O'Loughlin, E.; Larese-Casanova, P.; Scherer, M.; Cook, R. E. Green rust formation from the bioreduction of -FeOOH (lepidocrocite): Comparison of several *Shewanella* species. *Geomicrobiol. J.* **2007**, *24*, 211−230.
(55) Ruby, C.; Upadhyay, C.; Géhin, A.; Ona-Nguema, G.; Génin, J. M. In situ redox flexibility of FeII-III oxyhydroxycarbonate green rust and fougerite. *Environ. Sci. Technol.* **2006**, *40* (15), 4696−702.
(56) Bocher, F.; Géhin, A.; Ruby, C.; Ghanbaja, J.; Abdelmoula, M.; Génin, J.-M. R. Coprecipitation of Fe(II-III) hydroxycarbonate green rust stabilised by phosphate adsorption. *Solid State Sci.* **2004**, *6* (1), 117−124.
(57) Génin, J.-M. R.; Bourrié, G.; Trolard, F.; Abdelmoula, M.; Jaffrezic, A.; Refait, P.; Maitre, V.; Humbert, B.; Herbillon, A. Thermodynamic equilibria in aqueous suspensions of synthetic and natural Fe(II)−Fe(III) green rusts: Occurrences of the mineral in hydromorphic soils. *Environ. Sci. Technol.* **1998**, *32* (8), 1058−1068.
(58) Drissi, S. H.; Refait, P.; Abdelmoula, M.; Génin, J. M. R. The preparation and thermodynamic properties of Fe(II)-Fe(III) hydroxide-carbonate (green rust 1); Pourbaix diagram of iron in carbonate-containing aqueous media. *Corros. Sci.* **1995**, *37* (12), 2025−2041.
(59) Murad, E.; Taylor, R. M., The oxidation of hydroxycarbonate green rusts. In *Industrial Applications of the Mössbauer Effect*; Long, G. J., Stevens, J. G., Eds.; Plenum: New York, 1986; pp 585−593.
(60) Crocombette, J. P.; Pollak, M.; Jollet, F.; Thromat, N.; Gautier-Soyer, M. X-ray-absorption spectroscopy at the Fe $L_{2,3}$ threshold in iron oxides. *Phys. Rev. B* **1995**, *52* (5), 3143.
(61) Kukkadapu, R. K.; Zachara, J. M.; Fredrickson, J. K.; Kennedy, D. W. Biotransformation of two-line silica-ferrihydrite by a dissimilatory Fe(III)-reducing bacterium: Formation of carbonate green rust in the presence of phosphate. *Geochim. Cosmochim. Acta* **2004**, *68* (13), 2799−2814.
(62) Cornell, R. M.; Schwertmann, U. *The Iron Oxides - Structures, Properties, Reactions, Occurences And Uses*; Wiley-VCH Verlag: Weinheim, 2003.
(63) Refait, P. H.; Abdelmoula, M.; GÉnin, J. M. R. Mechanisms of formation and structure of green rust one in aqueous corrosion of iron in the presence of chloride ions. *Corros. Sci.* **1998**, *40* (9), 1547−1560.
(64) Randall, S. R.; Sherman, D. M.; Ragnarsdottir, K. V. Sorption of As(V) on green rust ($Fe_4(II)Fe_2(III)(OH)_{12}SO_4 \cdot 3H_2O$) and lepidocrocite ([gamma]-FeOOH): Surface complexes from EXAFS spectroscopy. *Geochim. Cosmochim. Acta* **2001**, *65* (7), 1015−1023.
(65) Putnis, A.; Putnis, C. V. The mechanism of reequilibration of solids in the presence of a fluid phase. *J. Solid State Chem.* **2007**, *180* (5), 1783−1786.
(66) Benali, O.; Abdelmoula, M.; Refait, P.; Génin, J.-M. R. Effect of orthophosphate on the oxidation products of Fe(II)-Fe(III) hydroxycarbonate: The transformation of green rust to ferrihydrite. *Geochim. Cosmochim. Acta* **2001**, *65* (11), 1715−1726.
(67) Roh, Y.; Lee, S. Y.; Elless, M. P. Characterization of corrosion products in the permeable reactive barriers. *Environ. Geol.* **2000**, *40* (1), 184−194.
(68) Bonin, P. M. L.; Odziemkowski, M. S.; Reardon, E. J.; Gillham, R. W. In-situ identification of carbonate-containing green rust on iron electrodes in solutions simulating groundwater. *J. Solution Chem.* **2000**, *29* (10), 1061−1074.
(69) Erbs, M.; Bruun Hansen, H. C.; Olsen, C. E. Reductive dechlorination of carbon tetrachloride using iron(II) iron(III) hydroxide sulfate (green rust). *Environ. Sci. Technol.* **1998**, *33* (2), 307−311.
(70) Myneni, S. C. B.; Tokunaga, T. K.; Brown, G. E. Abiotic selenium redox transformations in the presence of Fe(II,III) oxides. *Science* **1997**, *278* (5340), 1106−1109.
(71) Refait, P.; Simon, L.; Génin, J.-M. R. Reduction of SeO_4^{2-} anions and anoxic formation of iron(II)−iron(III) hydroxy-selenate green rust. *Environ. Sci. Technol.* **2000**, *34* (5), 819−825.
(72) O'Loughlin, E. J.; Kelly, S. D.; Cook, R. E.; Csencsits, R.; Kemner, K. M. Reduction of uranium(VI) by mixed iron(II)/iron(III) hydroxide (green rust): Formation of UO_2 nanoparticles. *Environ. Sci. Technol.* **2003**, *37* (4), 721−7.
(73) O'Loughlin, E. J.; Kelly, S. D.; Kemner, K. M.; Csencsits, R.; Cook, R. E. Reduction of Ag(I), Au(III), Cu(II), and Hg(II) by Fe(II)/Fe(III) hydroxysulfate green rust. *Chemosphere* **2003**, *53* (5), 437−46.
(74) Refait, P.; Génin, J. M. R. Mechanisms of oxidation of Ni(II)-Fe(II) hydroxides in chloride-containing aqueous media; role of the pyroaurite-type Ni-Fe hydroxychlorides. *Clay Miner.* **1997**, *32* (4), 597−613.
(75) Refait, P.; Abdelmoula, M.; Trolard, F.; Génin, J.-M. R.; Ehrhardt, J. J.; Bourrie, G.; Mossbauer, X. A. S. study of a green rust mineral; the partial substitution of Fe^{2+} by Mg^2. *Am. Mineral.* **2001**, *86* (5−6), 731−739.
(76) Wang, Y.; Morin, G.; Ona-Nguema, G.; Juillot, F.; Guyot, F.; Calas, G.; Brown, G. E. Evidence for different surface speciation of arsenite and arsenate on green rust: an EXAFS and XANES study. *Environ. Sci. Technol.* **2010**, *44* (1), 109−15.
(77) Génin, J.-M. R.; Abdelmoula, M.; Ruby, C.; Upadhyay, C. Speciation of iron; characterisation and structure of green rusts and FeII-III oxyhydroxycarbonate fougerite. *C. R. Geosci.* **2006**, *338* (6−7), 402−419.